Computational Biology and Chemistry 106 (2023) 107936

Contents lists available at ScienceDirect

Computational Biology and Chemistry

journal homepage: www.elsevier.com/locate/cbac

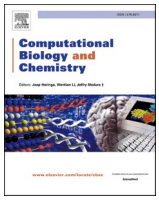

Theoretical investigation of hydroxylated analogues of valinomycin as potassium transporter

Lucia Sessa [a,b,*], Simona Concilio [a,b], Francesco Marrafino [a], Arkadeep Sarkar [a], Rosita Diana [c], Stefano Piotto [a,b]

[a] Department of Pharmacy, University of Salerno, Via Giovanni Paolo II 132, 84084 Fisciano, SA, Italy
[b] Bionam Research Centre for Biomaterials, University of Salerno, Via Giovanni Paolo II 132, 84084 Fisciano, SA, Italy
[c] Department of Agricultural Sciences, University of Naples Federico II, Via Università, 100, 80055 Portici, Italy

ARTICLE INFO

Keywords:
Valinomycin
Metadynamics
Hydroxylated VLM analogues
Free energy
Transition state

ABSTRACT

Valinomycin is a potent ionophore known for its ability to transport potassium ions across biological membranes. The study focuses on the hydroxylated analogues of valinomycin (HyVLMs) and compares their energy profiles and capabilities for transporting potassium ions across phospholipid membranes. Using metadynamics, we investigated the energy profiles of wild—type valinomycin (VLM_1) and its three hydroxylated analogues (VLM_2, VLM_3, and VLM_4). We observed that all analogues exhibited energy maxima in the centre of the membrane and preferred positions below the phospholipid heads. Furthermore, the entry barriers for membrane penetration were similar among the analogues, suggesting that the hydroxyl group did not significantly affect their passage through the membrane. Transition state calculations provided insights into the ability of valinomycin analogues to capture potassium ions, with VLM_4 showing the lowest activation energy and VLM_2 displaying the highest. Our findings contribute to understanding the mechanisms of potassium transport by valinomycin analogues and highlight their potential as ionophores. The presence of the hydroxyl group is of particular importance because it paves the way for subsequent chemical modifications and the synthesis of new antiviral agents with reduced intrinsic toxicity.

1. Introduction

Valinomycin is a nonribosomal peptide first isolated and characterised in 1955 from Streptomyces fulvissimus. Specifically, VLM is a cyclic depsipeptide consisting of D—valine, D—α-hydroxyvaleric, L—valine, and L—lactic acid in the cycle sequence [(L—Val — D—Hyv — D—Val — L—Lac)$_3$]. Valinomycin was initially discovered as an antibiotic compound that exhibited antibacterial effects against Mycobacterium tuberculosis (Brockmann and Schmidt-Kastner, 1955). Later, *in vitro* studies have shown that VLM exhibits a wide range of antibacterial activity. Cell growth inhibition has been extensively tested on several bacteria strains, particularly Gram—positive bacteria, such as Staphylococcus aureus (Tempelaars et al., 2011). However, none of the Gram—negative bacteria tested was inhibited by VLM. The lack of susceptibility of Gram—negative bacteria to VLM is attributed mainly to the outer membrane of the cell wall, which acts as a selective barrier by limiting access to the peptide (Ryabova et al., 1975).

Furthermore, VLM is the first naturally occurring compound identified as an ionophore with antibiotic function. VLM can selectively transport alkali metal ions across biological and synthetic membranes (Su et al., 2019). This ion transport property is mainly due to the formation of an ion—peptide complex. VLM forms stable complexes with K^+, Rb^+ and Cs^+, although with a definite preference for potassium (Ross et al., 2019). X—ray diffraction data of the valinomycin—K^+ complex revealed that the cation resides in the central cavity of the VLM ring and is coordinated with the oxygen atoms of the six ester carbonyls (Neupert-Laves and Dobler, 1975) (Fig. 1a). The cavity size is suitable for hosting a K^+ ion but no other metal ions in the cytoplasm, making the VLM an ionophore specific for potassium (Ross et al., 2019). It is well known that the valinomycin—K^+ complex can be incorporated into biological membranes, which allows K^+ transport across the phospholipid bilayer. VLM dissipates the potassium gradient across membranes, potentially killing bacterial cells (Leitch et al., 2013; Surewicz and Mantsch, 1988). The mechanism of action of VLM as a potassium ionophore within biological membranes is schematized in Fig. 1b (Huang et al., 2021).

* Corresponding author at: Department of Pharmacy, University of Salerno, Via Giovanni Paolo II 132, 84084 Fisciano, SA, Italy.
E-mail address: lucsessa@unisa.it (L. Sessa).

https://doi.org/10.1016/j.compbiolchem.2023.107936
Received 21 May 2023; Received in revised form 25 July 2023; Accepted 26 July 2023
Available online 28 July 2023

VLM is responsible for the dissipation of the mitochondrial membrane potential and the subsequent cell apoptosis (Inai et al., 1997); simultaneously, it is described as an inducer of uncoupling of cellular respiration and depolarization of mitochondria isolated *in vitro* (Furlong et al., 1998). In solution, VLM can assume different conformations depending on the polarity of the medium and the potassium ion concentration. The antibacterial action of VLM has been attributed to ionophore—mediated loss of K^+ from the bacterial cell, leading to impaired protein synthesis (Huang et al., 2021). The effectiveness of valinomycin is pH—dependent and influenced by the concentration of potassium ions in the cultivation medium.

A diverse spectrum of valinomycin biological activities was demonstrated, ranging from antifungal, antiviral, and insecticidal to antitumor efficacy. Membrane—active peptides and proteins have essential biological functions, such as electron and proton transfer, voltage—dependent ion translocation, drug direction and release, and antibiotic activity (Scrima et al., 2014; Sessa et al., 2020). VLM is a potent antiviral agent *in vitro* against various viruses, including coronaviruses, enteroviruses, and flaviviruses (Sandler et al., 2020; Zhang et al., 2020). Studies have shown that VLM was the most effective inhibitor against SARS and MERS, with a high potency against MERS—CoV (Fatoki et al., 2021; Huang et al., 2021; Wu et al., 2004). Recent studies have also demonstrated that VLM has a high binding affinity to SARS—CoV—2 proteins. However, its mechanism of action against SARS—CoV—2 is still unknown (Fatoki et al., 2021). In addition, its antitumor efficacy has been evaluated against multiple cancer cell lines (Inai et al., 1997).

Although it is not an FDA—approved antiviral drug for humans, modification of its structure may reduce drug toxicity while maintaining bioactivity *in vivo*. Structure—activity relationships studied with valinomycin analogues indicated that the cyclic 12–residue peptide is crucial for bioactivities. Changes to the valinomycin structure, such as altering the size of the rings or modifying the amino acid residues, significantly reduce its ability to form a stable complex with potassium ions, decreasing its antimicrobial activity (Shemyakin et al., 1973). Therefore, conjugating VLM with specific ligands that target diseased cells could be a highly effective approach to enhance its therapeutic potential while reducing its cytotoxicity (Srinivasarao and Low, 2017). By selectively delivering VLM to targeted cells, the treatment can be more efficient and minimize harm to healthy cells. This strategy is promising because it allows for the use of VLM's potent antimicrobial activity against specific disease—causing agents while underestimating its adverse effects on healthy cells. A recent study reported the synthesis of chemically modified hydroxylated VLM analogues carrying an OH group on the isopropyl side chain of a D—Hyi, D—Val, or L—Val residue (Fig. 2) (Annese et al., 2013). Hydroxylation is a well—known mechanism for modulating the physical state of the membrane (Friedman et al., 2018; Piotto et al., 2014; Piotto et al., 2018). Therefore, it opens the possibility of further chemical modification of VLM using the reactivity of the OH group. Annese et al. (Annese et al., 2013) evaluated the effect of OH group addition for various hydroxylated analogues (HyVLMs) on the bioenergetic parameters of rat liver—isolated mitochondria (RLM). The results of these studies clearly showed that HyVLMs are less bioactive than VLM. However, they retain the ability to chelate potassium ions, and the extent of the reduced bioactivity depends on the hydroxylation site (Annese et al., 2013). Adding an OH group on the side chain of D—Val and L—Val residues leads to derivatives that more closely resemble the behaviour of wild—type VLM. However, the decrease in bioactivity is exceptionally marked when hydroxylation involves the side chain of a D—Hyi residue.

We analysed several aspects concerning the impact of the hydroxyl group that need to be clarified to understand the mechanism of valinomycin and rationalise the activity of the analogues.

First, hydroxyl groups in valinomycin analogues can impact molecule solubility, potentially limiting their ability to cross the cell membrane. The log P value is a valuable metric for predicting a compound's solubility in different solvents. Therefore, the hydroxyl group's impact on valinomycin analogues' solubility should be considered in designing potential therapeutic agents.

Then, the presence of hydroxyl groups may alter the binding of valinomycin analogues to potassium ions. To study this aspect, the transition state of wild—type valinomycin in the bound and unbound state was analysed, and the orbitals involved in potassium complexation were identified. The differences among the four molecules offer insights into the potential effects of hydroxylation on the ion binding.

Finally, hydroxylation can affect the ability of valinomycin analogues to cross the cell membrane. The energy profile of membrane crossing for loaded and unloaded valinomycins was reconstructed using metadynamics.

Metadynamics is a computational technique widely used to study various molecular phenomena, including protein folding, ligand binding, and membrane transport. The method allows overcoming "slow" degrees of freedom, requiring currently inaccessible computational times to explore complex free energy landscapes in ordinary MD simulations. In addition, the technique involves using a bias potential to overcome energy barriers, which enables the system to explore a broader range of conformational space. The concept of metadynamics is to overcome barriers in the free energy landscape by defining one or multiple so—called collective variables (CVs) along which accelerated sampling is desired (Bussi and Laio, 2020). In the case of membrane—crossing peptides, one of the important collective variables to monitor during metadynamics simulations is the peptide's position along the membrane's Z—axis. This variable reflects the peptide's depth within the lipid bilayer and can help identify the pathways and energetics involved in peptide translocation across the membrane.

We performed a metadynamics study of VLM and HyVLM derivatives on a membrane model of POPC (palmitoyl—oleoyl—phosphatidylcholine), the most widely used component in model membranes (Sugita et al., 2021). Simulations allowed the reconstruction of the complete pathway for the VLM to leave the cytosol, cross the membrane surface,

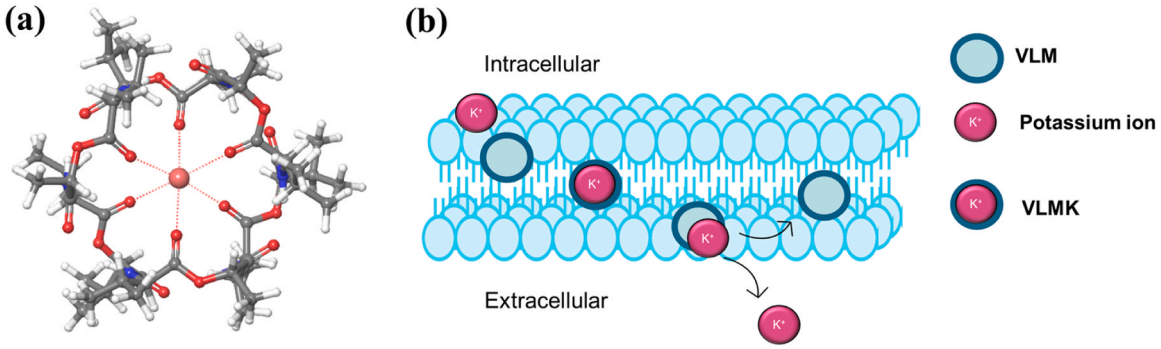

Fig. 1. (a) Valinomycin—K^+ complex. (b) valinomycin acts as potassium—selective ionophore.

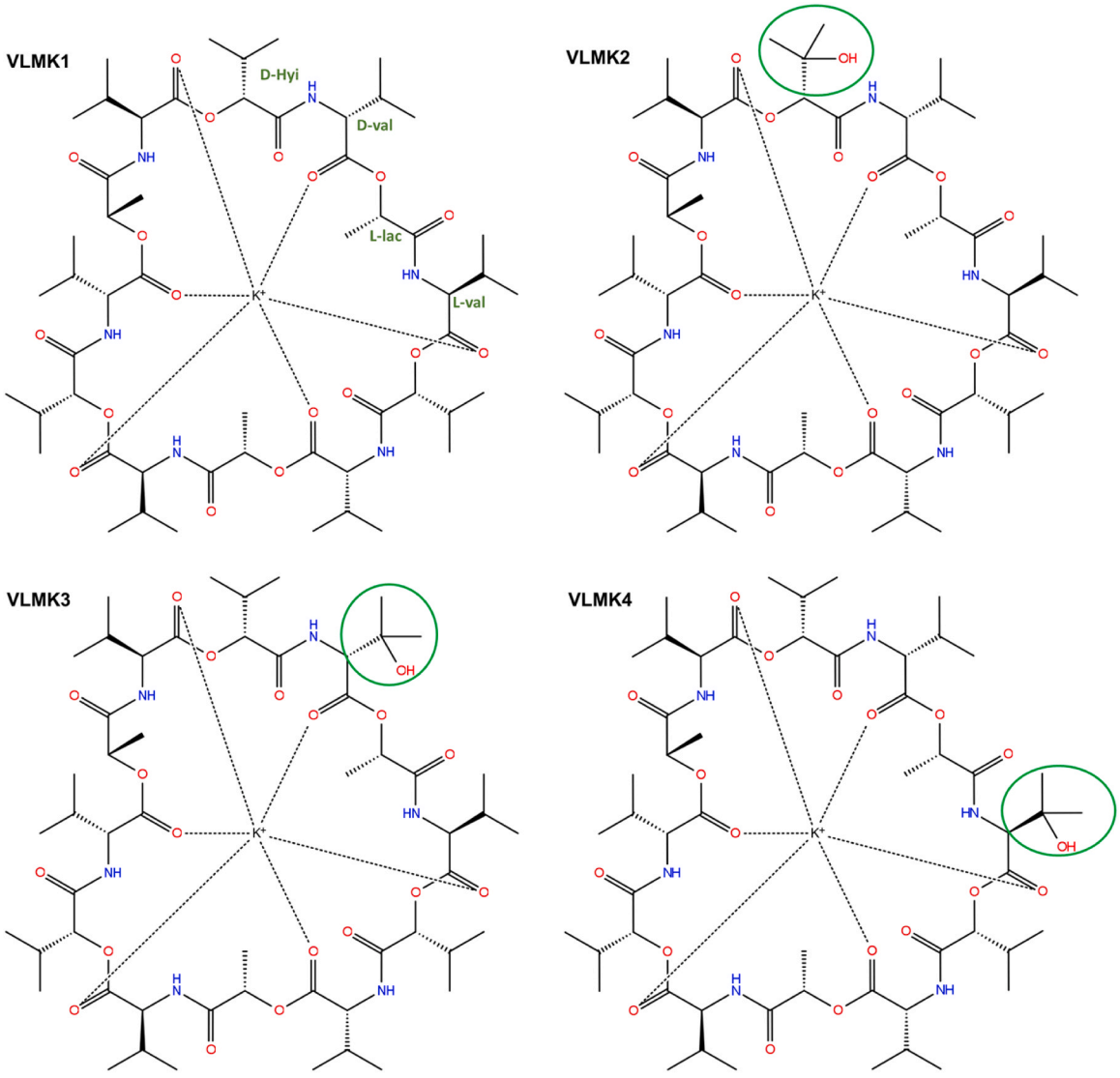

Fig. 2. VLM and hydroxylated analogues. VLMK_1 is the complex between VLM and K^+; a hydroxyl group was added on D—hydroxyvaleric acid for VLMK_2, on D—Valine for VLMK_3, and L—Valine for VLMK_4.

and position itself between lipid chains. These results can provide insights into potential modifications to VLM to improve membrane crossing and optimize the biological activity of valinomycin analogues. Overall, understanding the impact of hydroxyl groups on solubility, ion binding, and membrane crossing can aid in the rational design of more effective valinomycin—based therapeutic agents.

2. Materials and methods

2.1. System preparation

The structure of valinomycin complexed with a potassium ion, labelled VLMK_1, was downloaded from the Swiss—PdbViewer website (Guex et al., v4.1). The ionophore appears as a 36–member chain of amine and hydroxy acid residues that are able, by folding over the potassium ion, to expose hydrophobic portions outward. This transformation allows the VLM to cross a lipid bilayer quickly. Then, three hydroxylated analogues were prepared from the VLMK_1 structure. The geometry of all systems was optimised to avoid overlapping. The structures were minimised by running combined steepest descent and simulated annealing techniques using the software YASARA Structure 21.6.16 (Krieger and Vriend, 2014). More details on the protocol used are presented in Sessa et al. works (Sessa et al., 2020; Sessa et al., 2021).

The analogues were labelled: VLMK_2 (OH on D—hydroxyvaleric acid), VLMK_3 (OH on D—Valine) and VLMK_4 (OH on L—Valine), respectively. The four structures are shown in Fig. 2. The corresponding unloaded analogues non—complexing K^+ were labelled VLM_2, VLM_3, and VLM_4.

2.2. Computation of the free energy of valinomycin and its analogues

The different activity on cell membranes of valinomycin and its derivatives is attributed to their different penetration (and solubility) in the bilayer. We calculated the changes in free energy during passage through a membrane of 100 % POPC using metadynamics calculations. We analysed the four valinomycins with (VLMK_1–4) and without the K^+ ion (VLM_1–4). The energy profiles were then compared with those of the free potassium ion.

We employed GPU—accelerated Desmond software on an NVIDIA GeForce GTX 980 graphic card obtained through Desmond academic license (Bhachoo and Beuming, 2017; Bowers et al., 2006; Release, 2017). The parameters representing the height and width of the Gaussians were set as default, respectively, at 0.03 kcal/mol and 0.05 Å. RESPA integrator was used with a time step of 2.0 fs (Humphreys et al.,

1994). For coulombic interactions, short—range cutoff radius was defined at 9 Å. We used the Nose—Hoover chain thermostat (Hoover, 1985) at a temperature of 300 K and 1 atm with an isotropic Martyna—Tobias—Klein barostat (Martyna et al., 1994) with a relaxation time of 2.0 ps. For all simulations, the complex was first embedded in a 100 % POPC model membrane (Fig. S1). Next, the systems were solvated in an orthorhombic box (60x60x40 Å) using the TIP3P water model with 0.15 M NaCl to simulate the physiological concentration of salts in biological cells. The OPLS2005 force field implemented in Desmond was used to model the systems (Shivakumar et al., 2010). Finally, the systems were minimized and equilibrated at a temperature of 300 K and a pressure of 1.013 bar. A wall was placed in each run at 50 Å. The free energy profiles across the lipid bilayer were calculated using the projection of the position of the molecules on the axis orthogonal to the membrane as the collective variable (CV). The CV used in this work consists of the distance along the z—axis (defined as z—dist) between the centre of mass of the atoms of the VLM molecule (or analogues), excluding hydrogen atoms, and the centre of mass of the carbon atoms of the lipid tails of the membrane. The trajectory frames were recorded at intervals of 100 ps for a simulation time of 100 ns. For each system, we ran three metadynamics; each run shares the same starting point but uses a different random seed.

The one—dimension free energy profile (FEP) of each run (namely the primitive FEP) was calculated. The calculation of the primitive FEP of an individual run is part of the standard metadynamics in Desmond. We calculated the average FEP derived from a set of primitive FEP of three replicas (Fig. S2). We considered a CV range from 0 to 44 Å, then from the centre of the membrane to the aqueous region. For intervals of 2 Å, the free energy value was calculated following the procedure reported by Wang et al. (Wang et al., 2022).

To assess the convergence of the simulations for the wild—type VLM (both loaded and unloaded), we examined the similarity between the free energy profiles generated from simulation durations of 50 ns, 100 ns, and 200 ns. Therefore, all simulations reached convergence at least within a simulation time of 100 ns.

2.3. Transition state calculation

All the quantum mechanical calculations were carried out using the GUIDE plugin (Sarkar et al., 2023) for YASARA Suite (Krieger and Vriend, 2014). GUIDE is a plugin that enables users to perform ORCA Version 5.0.2 (Neese, 2012) and MOPAC2016, Version: 22.111 L (Stewart, 1990). We performed geometry optimization of hydroxylated analogues using PM7 semiempirical methods followed by DFT calculation using B3LYP functional and DEF2–SVP basis set information (Barabaś et al., 2019; Sarkar et al., 2023).

QM—based TS (quantum mechanical transition state) calculations were performed in vacuum using the semiempirical GFNn—xTB method (Bannwarth et al., 2019) using the GUIDE plugin. A fully hydrated membrane represents an extremely heterogeneous and anisotropic system that cannot be easily simulated using COSMO solvation. For this reason, it was decided to conduct this analysis in vacuum, although it represents a crude approximation of the real situation.

All the DFT levels (with B3LYP functional and DEF2–SVP basis set) geometry—optimized valinomycin analogues were considered the endpoint product for the TS calculation. In this study, we initiated the exploration of the valinomycin—K complex structure by first obtaining the DFT—optimized geometry of the system. The starting point is valinomycin obtained from the Swiss—PdbViewer website (Guex et al., v4.1). To build the endpoint, we moved 10 Å away from the potassium. Both structures have been optimized using the GFNn—xTB tight binding semiempirical QM method (Bannwarth et al., 2019).

We used the nudged elastic band method (NEB) for the TS calculations, setting the RMSD—push and pulling pathfinder values to 0.003 and −0.015, respectively (Dohm et al., 2020). This information was provided to the TS calculation as the pathfinder input file. Intrinsic bond orbitals (iboexp = 2) are generated using IboView (Knizia, 2013). The isosurfaces enclose 80 % of the total electron density.

2.4. Solubility descriptor

Octanol−water partition coefficients were calculated by Materials Studio 2020 using the ALogP function on the QSAR menu (Ghose et al., 1998). AlogP is a molecular descriptor related to the hydrophobic character of the molecule.

3. Results and discussion

AlogP is commonly utilized as a significant physicochemical parameter in drug discovery. It indicates a compound's capacity to cross biological barriers, particularly cell membranes composed primarily of lipids. Moreover, AlogP plays a crucial role in balancing a compound's solubility and permeability. Highly hydrophilic compounds may exhibit favourable solubility but often possess inadequate membrane permeability, constraining their effectiveness as therapeutic agents. The calculated AlogP values are 5.27 for VLM_1 and 4.11 for the three HyVLMs analogues. These results show that hydroxylation of valinomycin increases its solubility in water and leads to a reduction in the AlogP value. This reduction in logP is advantageous for oral drug administration, as it increases the likelihood that the compound will possess adequate membrane permeability (Lipinski et al., 2001). It is worth noting that cyclic peptides containing D-amino acids, such as cyclosporine, have been successfully administered orally despite their relatively high molecular weight and lipophilicity. Therefore, the hydroxylation-induced decrease in AlogP observed in the HyVLMs analogues may enhance their potential as oral therapeutic agents, offering improved solubility in water while still maintaining the capacity to cross biological barriers effectively.

3.1. Free energy profiles: comparison between loaded and unloaded wild—type VLM

The free energy profile was calculated by varying the distance between the centre of mass of valinomycin and that of the membrane.

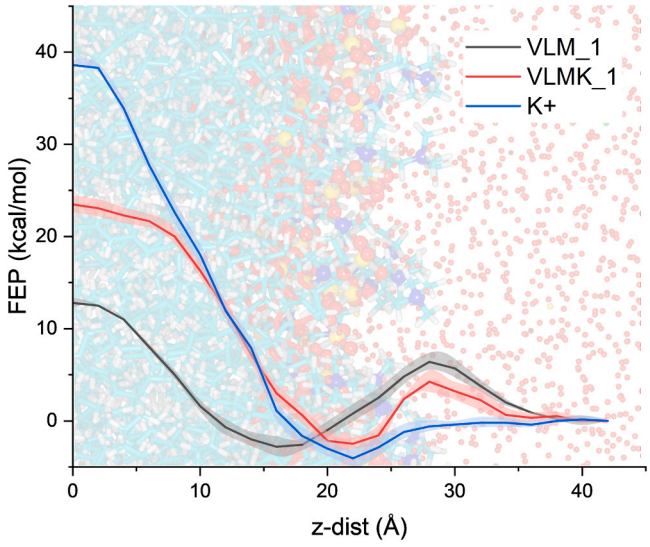

Fig. 3. Free energy profiles of the loaded and unloaded VLM (red and black lines, respectively) and potassium ions (blue line). The shadow under each curve indicates the error calculated by the primitive FEP. The approximate positions of lipid and solvent molecules are depicted in the background. Solvent molecules are shown as small red balls. The lipid leaflet molecules are drawn as a ball and stick model. The position of the phosphatidylcholine head is in the 18–28 Å zone.

(Fig. 3). On the x-axis of the graph is the z—dist. On the y—axis is the value of the free energy of the potassium ion or valinomycins. The zero of the z—dist axis corresponds to the centre of the phospholipid membrane. The overall membrane thickness (averaged among the phosphorous atoms on both membrane leaflets) is 38.7 ± 2.1 Å. The region at the interface, populated by the polar heads of POPC, is at a distance of about 20–30 Å. The region beyond 30 Å is cytosolic bulk.

The energy of the K^+ ion in bulk is set equal to 0 kcal/mol. Minimum energy is observed near the membrane surface due to electrostatic interactions with the zwitterionic lipid heads (blue line in Fig. 3). Inside the membrane, the energy of the potassium ion reaches a maximum of about 38 kcal/mol. In its energy profile, the potassium ion shows a minimum at 22 Å from the centre of the membrane, indicating a preference to reside near the phosphatidylcholine headgroups. As widely reported in the literature, the energy profile and the ΔG values confirm that cations must be transported across the non—polar region and released on the opposite side of a membrane (Su et al., 2021).

In bulk, VLM_1 uses six of its carbonyl groups and one of the ester oxygens to establish hydrogen bonds with water molecules (Fig. S3). Near the bilayer surface, ΔG increases and reaches an energy maximum (ΔG = 12.8 kcal/mol) in the membrane core. The relatively low energy barrier allows VLM_1 to move freely from one side of the membrane to the other. The energy profile of VLM_1 shows a minimum at 16 Å from the centre of the membrane, then below the lipid heads (black line in Fig. 3). This indicates that VLM can efficiently recruit a metal ion from the interphase and translocate it to the other side of the membrane. VLMK_1, being charged, has a maximum of about 23 kcal/mol in the centre of the membrane, and it slowly decreases, proceeding toward the water (red line in Fig. 3). Because of the shield offered by valinomycin, the presence of potassium significantly decreases the energy in the centre of the membrane; the energy is more than 15 kcal/mol lower than that of the potassium ion. However, the energy barrier to be overcome is much lower than for the isolated potassium ion not shielded by valinomycin. The energy barrier separating the two sides of the membrane is reduced by more than 3 times, allowing rapid and effective depolarization.

3.2. *Free energy profiles: comparison between VLM and its three hydroxylated analogues*

We compared the energy profiles of VLM_1 and its hydroxylated versions (Fig. 4a). In addition, we analysed the energy profiles of K^+—loaded valinomycins, denoted as VLMK_ and shown in Fig. 4b. For easier comparison of the free energy profiles, the energy was set to zero in bulk (z = 40 Å).

The results observed in Fig. 4a indicate the presence of a significant energy barrier at the centre of the membrane. Compared to VLM_1, the unloaded analogues exhibit more pronounced energy maxima in the membrane. The centre of the membrane corresponds to z = 0 Å, where the free energy barrier increases from 12.8 (of VLM_1) to 18.8 kcal/mol for the hydroxylated analogues. The higher energy belongs to VLM_2, implicating that it is more challenging to cross the membrane for VLM_2 than the other analogues. All VLMs analogues showed interesting behaviour, with a minimum at about 16 Å distance from the centre of the membrane, just below the phospholipid heads. In addition, another energy barrier was observed near the interface between the membrane and water. We set the entry barrier as the energy required for the VLMs to move from the aqueous environment to the lipid head region, as presented in Table 1. The barrier at the centre of the membrane corresponds to the difference between the maximum (at 0 Å) and the

Table 1
The free energy costs of VLMs.

Molecule	ΔG (kcal/mol)[a]	
	Barrier at the membrane centre	Entry barrier
K^+	42.7 ± 1.1	4.1 ± 1.0
VLM_1	15.6 ± 1.2	9.2 ± 1.4
VLM_2	20.3 ± 1.0	10.0 ± 1.0
VLM_3	16.7 ± 0.8	9.4 ± 0.8
VLM_4	17.5 ± 1.1	9.5 ± 1.0
VLMK_1	26.0 ± 1.1	6.7 ± 1.3
VLMK_2	28.9 ± 1.2	5.5 ± 1.2
VLMK_3	27.2 ± 1.1	7.1 ± 1.0
VLMK_4	27.6 ± 1.0	6.8 ± 1.2

[a] The free energy was obtained by metadynamics. The error reported is the standard deviation of the mean of 3 independent simulations with 3 different seeds.

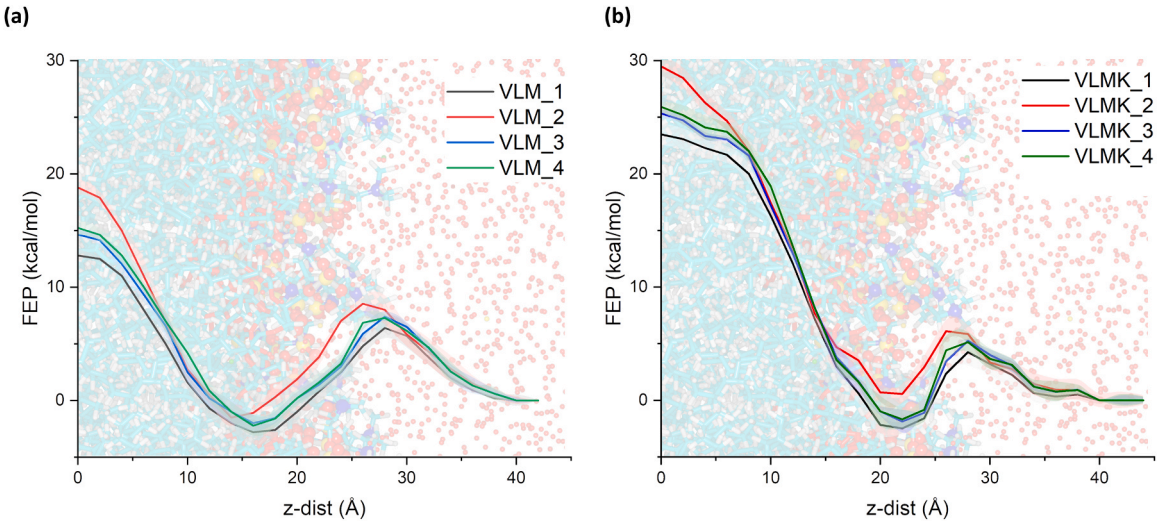

Fig. 4. Comparison among the energy profile of the wild—type VLM_1 (black line) and the three hydroxylated analogues (VLM_2 red line, VLM_3 blue line and VLM_4 green line) **(a)**; and of the loaded VLMK_1 (black line) and its three hydroxylated analogues (VLMK_2 red line, VLMK_3 blue line and VLMK_4 green line) **(b)**. In both panels, the shadow under each curve indicates the error calculated by the primitive FEP. The approximate positions of lipid and solvent molecules are depicted in the background. Solvent molecules are shown as small red balls. The lipid leaflet molecules are drawn as a ball and stick model. The position of the phosphatidylcholine head is approximately at 18–28 Å from the centre of the membrane.

minimum energy at about 16 Å (see Fig. 4a).

The analogues studied show remarkable similarities in their energy profiles. The energy patterns shown in Fig. 4a indicate an energy maximum in the centre of the membrane and a preferred position below the phospholipid heads. Furthermore, a closer examination of Table 1 reveals that the input barrier values for each analogue are highly similar. Considering the high structural similarity between the analogues, these results are not unexpected. The molecules share common structural motifs, differing mainly in the presence of an additional hydroxyl group. However, VLM_2 has the highest barrier to entry among all the analogues studied. In contrast, VLM_3 and VLM_4 show comparable barriers to entry, with a trend more similar to that of the wild—type.

The energy profile of the four complexes is shown in Fig. 4b. The K^+—loaded hydroxylated analogues show high energy at the membrane's centre, with a free energy maximum between 23 and 30 kcal/mol. On the other hand, the loaded VLMK structures exhibit a common trend that includes a minimum near the membrane surface. This energetically favourable position facilitates the release of potassium ions into the cytosol. Despite showing a slightly higher energy barrier in the membrane (approximately 29 kcal/mol), also the analogue VLMK_2 is still able to fulfil its function as a potassium transporter in the membrane. It is found that all four compounds significantly decrease the energy barrier required for the passage of metal ions across the membrane. The mechanism by which VLM depolarizes the membrane consists of three successive steps. The first step involves the insertion of the valinomycin into the membrane, and as mentioned above, all analogues can insert into the bilayer (Fig. 4a). The second step involves valinomycin getting close enough to the cytosol to capture a potassium ion. Finally, the third step is valinomycin coordinated with the potassium ion to cross the membrane (Fig. 4b). The differences between the membrane entry barriers and the barriers at the membrane centre for the four analogues are minimal. Therefore, the presence of the hydroxyl group does not seem to affect the passage of valinomycin through the membrane significantly (Table S1 for p-values comparison).

3.3. Transition state calculation of VLMK and HyVLMK complexes

Transition state (TS) calculation is an essential parameter for understanding the mechanisms of any chemical reactions (Madarász et al., 2016). TS calculations can identify the most favourable reaction path, the energy barriers for each reaction step, and the energy landscape of the reaction. The results of TS calculations can be further used to predict reaction rates, reaction selectivity, and the overall yield of the reaction (Zinovjev et al., 2018).

The reaction coordinates represent the progression of the reaction from the reactant state ($VLM\__i + K^+$) to the product state ($VLMK\_i$). We denote both systems as VLM_*i* and VLMK_*i*, where "$_i$" goes from 1 to 4 to distinguish the four analogues. The reaction coordinates represent the various steps involved in the complexation process (Fig. 5a).

TS analysis shows that the valinomycin—potassium ion complex is always favoured energetically (see Fig. 5a and Table 2). In the initial stage, the potassium ion approaches valinomycin (VLM_i) to form a temporary encounter complex characterized by weak interactions and high translational and rotational freedom. Successively, the encounter complex undergoes a transition state in which the potassium ion begins to coordinate with valinomycin binding sites, forming the valinomycin-potassium complex. This transition state represents a local energy maximum on the reaction pathway. Finally, the complexation process progresses to the product state when the potassium ion becomes fully coordinated with valinomycin ($VLMK\_i$).

The energy barrier to overcome (activation energy, E_{act}) required to effectively coordinate the potassium ion is highest in VLM_2, being nearly 40 kcal/mol, whereas it is lowest in VLM_3 and VLM_4. This disparity in activation energy results in an enhanced ability for VLM_3 and VLM_4 to coordinate the potassium ion with their respective hydroxyl groups. Based on this finding, we can infer that hydroxylation of D-Valine or L-Valine leads to a reduction in the activation barrier, while hydroxylation of D-hydroxyvaleric acid appears to raise the activation barrier.

Table 2
Calculated activation energies.

System	ΔG (kcal/mol)±1.5[a]	E_{act} (kcal/mol)±0.6[b]
VLM_1	-60.1	23.5
VLM_2	-56.8	37.8
VLM_3	-66.2	10.5
VLM_4	-59.3	11.8

[a] Standard error of the protocols (Dohm et al., 2020)
[b] Standard error of the protocols (Bannwarth et al., 2021).

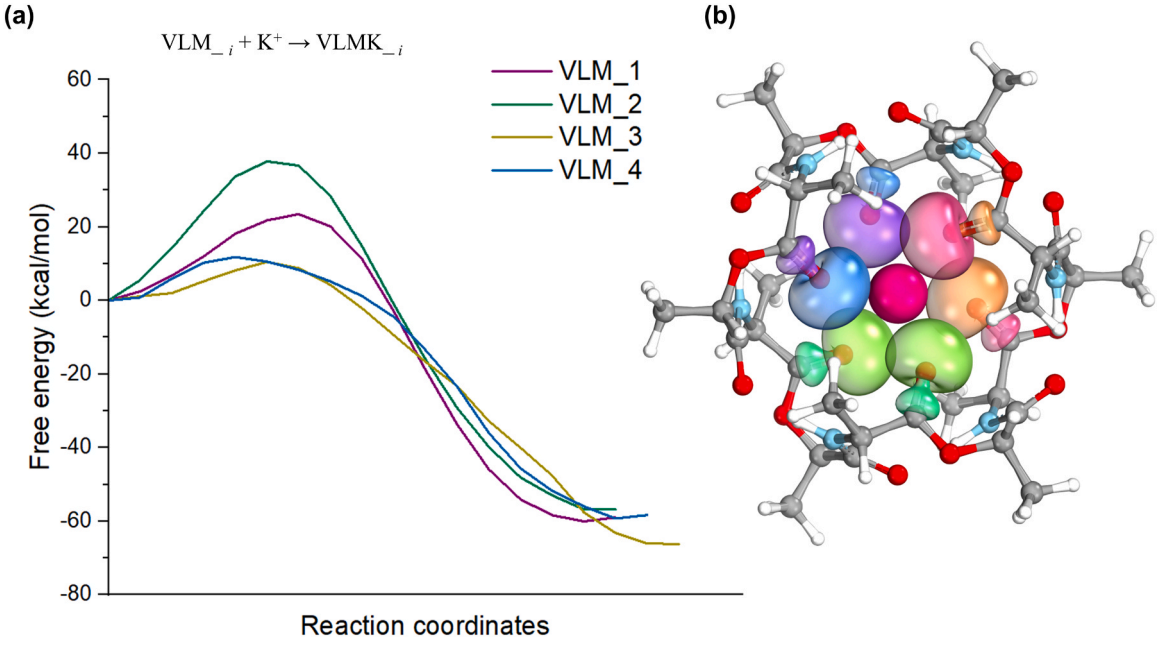

Fig. 5. **(a)** Reaction coordinates for potassium complexation **(b)** Intrinsic Orbitals of VLMK_1 at minimum energy.

Overall, our TS calculations provide insight into the ability of valinomycins to capture potassium ions, highlighting the differences in activation energy among the analogues and their potential as metal binders.

The conformational changes undergone by VLM_1 during the complexation process of the potassium ion are shown in Fig. S4. The potassium ion is located away from the valinomycin in the initial state. During the complexation process, the potassium ion is captured within the molecule. The key to this process is the coordination of the potassium ion with six oxygen atoms in the molecule. To get a qualitative picture of the complexation of the potassium ion, we showed the intrinsic bonding orbitals (IBOs) (Fig. 5b). Analysis of the IBOs of the oxygen atoms involved in the interaction with potassium indicates a 2 per cent contribution for the potassium atom per metal—oxygen interaction. The most relevant structures along the TS are shown in Fig. S4 to compare the four analogues better.

4. Conclusions

The wild—type VLM (VLM_1) is the most effective ionophore, and studies have shown that it can transfer large amounts of ions across phospholipid membranes. The desire to reduce its intrinsic toxicity led to the evaluation of chemical modifications, such as site-specific hydroxylation of VLM, which could be a quick way to tune the bioactivity of the wild-type molecule finely. In this work, we considered three hydroxylated analogues: VLM_2, VLM_3, and VLM_4. Metadynamics allowed the energy profile of the wild—type molecule and its hydroxylated analogues in the cytosolic bulk and membrane to be evaluated. VLM_1 easily penetrates the membrane due to the change in the polarity of its outer surface. VLM_1 remains between the phospholipid heads until it captures a K^+ ion, which is present in high concentrations on the cytosolic side. Once the cation has been chelated, VLMK_1 easily crosses the POPC membrane. The concentration gradient of potassium ions drives the crossing. VLM can significantly reduce the energy required to cross the membrane and leads to rapid release of ions inside the mitochondrion. The energy profile of the four molecules reveals that among the hydroxylated analogues, VLMK_3 and VLMK_4 are those with the most regular energy profile, suggesting high bioactivity. On the other hand, VLM_2 is an analogue that shows the most difficulty in recovering K^+ ions from the cytosol and crossing the membrane. *In vitro* analysis revealed the lowest bioactivity among the four molecules compared.

We used transition state calculations to evaluate the ability of the valinomycins to capture potassium ions. The complexed form was found to have lower free energy than the potassium—free forms in all four cases. VLM_4 and VLM_3 had the lowest activation energy, suggesting they might be the more efficient transporters of potassium ions. VLM_2 had the highest activation energy and might be the least efficient transporter.

The initial hypotheses proposed in this study included the possibility that the different activity of the analogues was related to solubility, ability to shuttle in the membrane, or ability to complex potassium. Our results suggest that the hydroxylation has no effect on membrane permeation and the latter hypothesis is the most plausible explanation. The presence of an additional hydroxyl group on the residues D-Valine for VLMK_3 and L-Valine for VLMK_4 drives the complexation of potassium by steering the ion towards the carbonyl groups responsible for hexa-coordination. In addition, the hydroxyl group plays a crucial role in facilitating future chemical modifications and developing potential new active molecules. This versatility allows researchers to finely tune the bioactivity of the molecule and explore different structural variations.

It is important to note that this conclusion was drawn based on experiments conducted on model POPC membranes, and that the calculations of complex formation in this study were only investigated in vacuum. Although these membranes are an extreme simplification of real cell membranes, they have been widely used in previous studies and provide valuable insights into the properties and behaviour of analogues. However, further studies using more complex membrane models, more detailed potassium complexation analysis and *in vitro* or *in vivo* experiments are needed to validate these results fully.

Although the mechanism of action of VLM in the treatment of SARS—CoV—2 has not yet been elucidated, considering its higher bioactivity, the analogue VLMK_3 is of particular interest. Its lower cytotoxicity *in vitro* would make it an ideal candidate for developing and optimising guide compounds for synthesising analogues with potential antiviral activity for therapy to benefit COVID—19 patients.

Funding

This research was funded by POR CAMPANIA FESR 2014/2020 project MIND: Molecules Inhibiting Neurological Diseases, CUP B31B19001540007. L.S. was financed by project PON 2014-2020-Az. IV.4 e IV.6.

CRediT authorship contribution statement

Lucia Sessa: Conceived the idea, Wrote the paper, Carried out the metadynamics simulations and analyzed the results. **Simona Concilio:** Wrote the paper, Collected the data. **Francesco Marrafino:** Wrote the paper, Performed the analysis. **Arkadeep Sarkar:** Carried out the DFT calculations and obtained the results. **Rosita Diana:** Performed the analysis. Stefano Piotto: Conceived the idea, Wrote the paper, Analyzed the results.

Declaration of Competing Interest

The authors declare that they have no known competing financial interests or personal relationships that could have appeared to influence the work reported in this paper.

Appendix A. Supporting information

Supplementary data associated with this article can be found in the online version at doi:10.1016/j.compbiolchem.2023.107936.

References

Annese, C., Abbrescia, D.I., Catucci, L., D'Accolti, L., Denora, N., Fanizza, I., Fusco, C., La Piana, G., 2013. Site-dependent biological activity of valinomycin analogs bearing derivatizable hydroxyl sites. J. Pept. Sci. 19 (12), 751–757. https://doi.org/10.1002/psc.2571.

Bannwarth, C., Ehlert, S., Grimme, S., 2019. GFN2-xTB—an accurate and broadly parametrized self-consistent tight-binding quantum chemical method with multipole electrostatics and density-dependent dispersion contributions. J. Chem. Theory Comput. 15 (3), 1652–1671. https://doi.org/10.1021/acs.jctc.8b01176.

Bannwarth, C., Caldeweyher, E., Ehlert, S., Hansen, A., Pracht, P., Seibert, J., Spicher, S., Grimme, S., 2021. Extended tight-binding quantum chemistry methods. Wiley Interdiscip. Rev.: Comput. Mol. Sci. 11 (2), e1493.

Barabaś, A., Jagiełło, K., Rybińska-Fryca, A., Dąbrowska, A.M., Puzyn, T., 2019. How the configurational changes influence on molecular characteristics. The alkyl 3-azido-2,3-dideoxy-D-hexopyranosides - Theoretical approach. Carbohydr. Res. 481, 72–79. https://doi.org/10.1016/j.carres.2019.06.012.

Bhachoo, J., Beuming, T., 2017. Investigating Protein–Peptide Interactions Using the Schrödinger Computational Suite. In: Schueler-Furman, O., London, N. (Eds.), Modeling Peptide-Protein Interactions: Methods and Protocols. Springer New York, New York, NY, pp. 235–254.

Bowers, K.J., Chow, E., Xu, H., Dror, R.O., Eastwood, M.P., Gregersen, B.A., Klepeis, J.L., Kolossvary, I., Moraes, M.A., Sacerdoti, F.D. *Scalable algorithms for molecular dynamics simulations on commodity clusters*, 2006, pp 84-es, 10.1145/1188455.1188544.

Brockmann, H., Schmidt-Kastner, G., 1955. Valinomycin I, XXVII. Mitteil. über antibiotica aus actinomyceten. Chem. Ber. 88 (1), 57–61. https://doi.org/10.1002/cber.19550880111.

Bussi, G., Laio, A., 2020. Using metadynamics to explore complex free-energy landscapes. Nat. Rev. Phys. 2 (4), 200–212. https://doi.org/10.1038/s42254-020-0153-0.

Dohm, S., Bursch, M., Hansen, A., Grimme, S., 2020. Semiautomated transition state localization for organometallic complexes with semiempirical quantum chemical

methods. J. Chem. Theory Comput. 16 (3), 2002–2012. https://doi.org/10.1021/acs.jctc.9b01266.
Fatoki, T.H., Ibraheem, O., Ogunyemi, I.O., Akinmoladun, A.C., Ugboko, H.U., Adeseko, C.J., Awofisayo, O.A., Olusegun, S.J., Enibukun, J.M., 2021. Network analysis, sequence and structure dynamics of key proteins of coronavirus and human host, and molecular docking of selected phytochemicals of nine medicinal plants. J. Biomol. Struct. Dyn. 39 (16), 6195–6217. https://doi.org/10.1080/07391102.2020.1794971.
Friedman, R., Khalid, S., Aponte-Santamaría, C., Arutyunova, E., Becker, M., Boyd, K.J., Christensen, M., Coimbra, J.T.S., Concilio, S., Daday, C., van Eerden, F.J., Fernandes, P.A., Gräter, F., Hakobyan, D., Heuer, A., Karathanou, K., Keller, F., Lemieux, M.J., Marrink, S.J., May, E.R., Mazumdar, A., Naftalin, R., Pickholz, M., Piotto, S., Pohl, P., Quinn, P., Ramos, M.J., Schiøtt, B., Sengupta, D., Sessa, L., Vanni, S., Zeppelin, T., Zoni, V., Bondar, A.N., Domene, C., 2018. Understanding conformational dynamics of complex lipid mixtures relevant to biology. J. Membr. Biol. 251 (5–6), 609–631. https://doi.org/10.1007/s00232-018-0050-y.
Furlong, I.J., Mediavilla, C.L., Ascaso, R., Rivas, A.L., Collins, M.K., 1998. Induction of apoptosis by valinomycin: mitochondrial permeability transition causes intracellular acidification. Cell Death Differ. 5 (3), 214–221. https://doi.org/10.1038/sj.cdd.4400335.
Ghose, A.K., Viswanadhan, V.N., Wendoloski, J.J., 1998. Prediction of hydrophobic (Lipophilic) properties of small organic molecules using fragmental methods: an analysis of ALOGP and CLOGP methods. J. Phys. Chem. A 102 (21), 3762–3772. https://doi.org/10.1021/jp980230o.
Guex, N., Diemand, A., Peitsch, M.C., Schwede, T. *Swiss-PdbViewer aka DeepView*, v4.1.
Hoover, W.G., 1985. Canonical dynamics: equilibrium phase-space distributions. Phys. Rev. A 31 (3), 1695–1697. https://doi.org/10.1103/PhysRevA.31.1695.
Huang, S., Liu, Y., Liu, W.-Q., Neubauer, P., Li, J., 2021. The Nonribosomal peptide valinomycin: from discovery to bioactivity and biosynthesis. Microorganisms 9 (4), 780. https://doi.org/10.3390/microorganisms9040780.
Humphreys, D.D., Friesner, R.A., Berne, B.J., 1994. A multiple-time-step molecular dynamics algorithm for macromolecules. J. Phys. Chem. 98 (27), 6885–6892. https://doi.org/10.1021/j100078a035.
Inai, Y., Yabuki, M., Kanno, T., Akiyama, J., Yasuda, T., Utsumi, K., 1997. Valinomycin induces apoptosis of ascites hepatoma cells (AH-130) in relation to mitochondrial membrane potential. Cell Struct. Funct. 22 (5), 555–563. https://doi.org/10.1247/csf.22.555.
Knizia, G., 2013. Intrinsic atomic orbitals: an unbiased bridge between quantum theory and chemical concepts. J. Chem. Theory Comput. 9 (11), 4834–4843. https://doi.org/10.1021/ct400687b.
Krieger, E., Vriend, G., 2014. YASARA View—molecular graphics for all devices—from smartphones to workstations. Bioinformatics 30 (20), 2981–2982. https://doi.org/10.1093/bioinformatics/btu426.
Leitch, J.J., Brosseau, C.L., Roscoe, S.G., Bessonov, K., Dutcher, J.R., Lipkowski, J., 2013. Electrochemical and PM-IRRAS characterization of cholera toxin binding at a model biological membrane. Langmuir 29 (3), 965–976. https://doi.org/10.1021/la304939k.
Lipinski, C.A., Lombardo, F., Dominy, B.W., Feeney, P.J., 2001. Experimental and computational approaches to estimate solubility and permeability in drug discovery and development settings. Adv. Drug Deliv. Rev. 46 (1–3), 3–26. https://doi.org/10.1016/s0169-409x(00)00129-0.
Madarász, A.D.M., Berta, D.N., Paton, R.S., 2016. Development of a true transition state force field from quantum mechanical calculations. J. Chem. Theory Comput. 12 (4), 1833–1844. https://doi.org/10.1021/acs.jctc.5b01237.
Martyna, G.J., Tobias, D.J., Klein, M.L., 1994. Constant pressure molecular dynamics algorithms. J. Chem. Phys. 101 (5), 4177–4189. https://doi.org/10.1063/1.467468.
Neese, F., 2012. The ORCA program system. Wiley Interdiscip. Rev.: Comput. Mol. Sci. 2 (1), 73–78. https://doi.org/10.1002/wcms.81.
Neupert-Laves, K., Dobler, M., 1975. The crystal structure of a K+ complex of valinomycin. Helv. Chim. Acta 58 (2), 432–442. https://doi.org/10.1002/hlca.19750580212.
Piotto, S., Trapani, A., Bianchino, E., Ibarguren, M., López, D.J., Busquets, X., Concilio, S., 2014. The effect of hydroxylated fatty acid-containing phospholipids in the remodeling of lipid membranes. ,1838 Biochim. Et. Biophys. Acta - Biomembr. 6, 1509–1517. https://doi.org/10.1016/j.bbamem.2014.01.014.
Piotto, S., Di Biasi, L., Sessa, L., Concilio, S., 2018. Transmembrane peptides as sensors of the membrane physical state, 6, MAY Front. Phys.. https://doi.org/10.3389/fphy.2018.00048.
Release, S. *Desmond molecular dynamics system, DE Shaw research, New York, NY, 2017*, Maestro-Desmond Interoperability Tools, Schrödinger, New York, NY 2017.
Ross, E.E., Hoag, B., Joslin, I., Johnston, T., 2019. Measurements of ion binding to lipid-hosted ionophores by affinity chromatography. Langmuir 35 (29), 9410–9421. https://doi.org/10.1021/acs.langmuir.9b01301.
Ryabova, I., Gorneva, G., Ovchinnikov, Y.A., 1975. Effect of valinomycin on ion transport in bacterial cells and on bacterial growth. Biochim. Et. Biophys. Acta (BBA)-Biomembr. 401 (1), 109–118. https://doi.org/10.1016/0005-2736(75)90345-4.
Sandler, Z.J., Firpo, M.R., Omoba, O.S., Vu, M.N., Menachery, V.D., Mounce, B.C., 2020. Novel ionophores active against La Crosse virus identified through rapid antiviral screening. Antimicrob. Agents Chemother. 64 (6), e00086–00020. https://doi.org/10.1128/AAC.00086-20.
Sarkar, A., Sessa, L., Marrafino, F., Piotto, S., 2023. GUIDE: A GUI for automated quantum chemistry calculations. J. Comput. Chem. 1–7. https://doi.org/10.1002/jcc.27177.
Scrima, M., Di Marino, S., Grimaldi, M., Campana, F., Vitiello, G., Piotto, S.P., D'Errico, G., D'Ursi, A.M., 2014. Structural features of the C8 antiviral peptide in a membrane-mimicking environment. ,1838 Biochim. Et. Biophys. Acta - Biomembr. 3, 1010–1018. https://doi.org/10.1016/j.bbamem.2013.12.010.
Sessa, L., Concilio, S., Walde, P., Robinson, T., Dittrich, P.S., Porta, A., Panunzi, B., Caruso, U., Piotto, S., 2020. Study of the interaction of a novel semi-synthetic peptide with model lipid membranes. Membranes 10 (10), 1–15. https://doi.org/10.3390/membranes10100294.
Sessa, L., Nardiello, A.M., Santoro, J., Concilio, S., Piotto, S., 2021. Hydroxylated fatty acids: The role of the sphingomyelin synthase and the origin of selectivity. Membranes 11 (10), 787. https://doi.org/10.3390/membranes11100787.
Shemyakin, M.M., Vinogradova, E.I., Ryabova, I.D., Fonina, L.A., Sanasaryan, A.A., 1973. Relationship between structure, stability of potassium complexes, and antimicrobial activity in a series of analogs of valinomycin. Chem. Nat. Compd. 9 (2), 229–234. https://doi.org/10.1007/BF00563351.
Shivakumar, D., Williams, J., Wu, Y., Damm, W., Shelley, J., Sherman, W., 2010. Prediction of absolute solvation free energies using molecular dynamics free energy perturbation and the OPLS force field. J. Chem. Theory Comput. 6 (5), 1509–1519. https://doi.org/10.1021/ct900587b.
Srinivasarao, M., Low, P.S., 2017. Ligand-targeted drug delivery. Chem. Rev. 117 (19), 12133–12164. https://doi.org/10.1021/acs.chemrev.7b00013.
Stewart, J.J., 1990. MOPAC: a semiempirical molecular orbital program. J. Comput. -Aided Mol. Des. 4 (1), 1–103.
Su, Z., Ran, X., Leitch, J.J., Schwan, A.L., Faragher, R., Lipkowski, J., 2019. How valinomycin ionophores enter and transport K+ across model lipid bilayer membranes. Langmuir 35 (51), 16935–16943. https://doi.org/10.1021/acs.langmuir.9b03064.
Su, Z., Leitch, J.J., Sek, S., Lipkowski, J., 2021. Ion-pairing mechanism for the valinomycin-mediated transport of potassium ions across phospholipid bilayers. Langmuir 37 (31), 9613–9621. https://doi.org/10.1021/acs.langmuir.1c01500.
Sugita, M., Sugiyama, S., Fujie, T., Yoshikawa, Y., Yanagisawa, K., Ohue, M., Akiyama, Y., 2021. Large-scale membrane permeability prediction of cyclic peptides crossing a lipid bilayer based on enhanced sampling molecular dynamics simulations. J. Chem. Inf. Model. 61 (7), 3681–3695. https://doi.org/10.1021/acs.jcim.1c00380.
Surewicz, W.K., Mantsch, H.H., 1988. New insight into protein secondary structure from resolution-enhanced infrared spectra. Biochim. Et. Biophys. Acta (BBA)-Protein Struct. Mol. Enzymol. 952, 115–130. https://doi.org/10.1016/0167-4838(88)90107-0.
Tempelaars, M.H., Rodrigues, S., Abee, T., 2011. Comparative analysis of antimicrobial activities of valinomycin and cereulide, the Bacillus cereus emetic toxin. Appl. Environ. Microbiol. 77 (8), 2755–2762. https://doi.org/10.1128/aem.02671-10.
Wang, J., Ishchenko, A., Zhang, W., Razavi, A., Langley, D., 2022. A highly accurate metadynamics-based Dissociation Free Energy method to calculate protein–protein and protein–ligand binding potencies. Sci. Rep. 12 (1), 2024. https://doi.org/10.1038/s41598-022-05875-8.
Wu, C.-Y., Jan, J.-T., Ma, S.-H., Kuo, C.-J., Juan, H.-F., Cheng, Y.-S.E., Hsu, H.-H., Huang, H.-C., Wu, D., Brik, A., 2004. Small molecules targeting severe acute respiratory syndrome human coronavirus. Proc. Natl. Acad. Sci. 101 (27), 10012–10017. https://doi.org/10.1073/pnas.0403596101.
Zhang, D., Ma, Z., Chen, H., Lu, Y., Chen, X., 2020. Valinomycin as a potential antiviral agent against coronaviruses: a review. Biomed. J. 43 (5), 414–423. https://doi.org/10.1016/j.bj.2020.08.006.
Zinovjev, K., Tuñón, I., 2018. Reaction coordinates and transition states in enzymatic catalysis. Wiley Interdiscip. Rev.: Comput. Mol. Sci. 8 (1), e1329 https://doi.org/10.1002/wcms.1329.